Spectrochimica Acta Part A: Molecular and Biomolecular Spectroscopy 122 (2014) 273–282

Contents lists available at ScienceDirect

Spectrochimica Acta Part A: Molecular and Biomolecular Spectroscopy

journal homepage: www.elsevier.com/locate/saa

Heterotrimetallic Ru(II)/Pd(II)/Ru(II) complexes: Synthesis, crystalstructure, spectral characterization, DFT calculation and antimicrobial study

Mousa Al-Noaimi [a,*], Ayman Nafady [b], Ismail Warad [c,*], Rwaida Alshwafy [d], Ahmad Husein [c], Wamidh H. Talib [e], Taibi Ben Hadda [f]

[a] Department of Chemistry, Hashemite University, P.O. Box 150459, Zarqa 13115, Jordan
[b] Department of Chemistry, College of Science, King Saud University, P.O. Box 2455, Riyadh 11451, Saudi Arabia
[c] Department of Chemistry, AN-Najah National University, Nablus, Occupied Palestinian Territory
[d] Department of Chemistry, College of Science, Taiz University, P.O. Box 6803, Republic of Yemen
[e] Department of Clinical Pharmacy and Therapeutics, Applied Science University, Amman 11931, Jordan
[f] Laboratoire LCM, Faculty of Sciences, University Mohammed 1[er], Oujda 60000, Morocco

HIGHLIGHTS

- Mononuclear Ru(II) and heterotrimetallic Ru(II)–Pd(II)–Ru(II) complexes are synthesized.
- The progress of the reactions was monitored by ^{31}P{1H} NMR and FTIR.
- The absorption spectrum was modeled by TD-DFT.
- Heterotrimetallic complexes exhibit high antibacterial and antifungal a inhibitory activity.

GRAPHICAL ABSTRACT

New ruthenium(II) mononuculear complexes of the type $[RuCl_2(PPh_3)_2(\eta^2\text{-triamine})]$ (**2**) $[RuCl(PPh_3)_2(\eta^2\text{-triamine})]Cl$ (**5**) (triemine = N^1-(2-aminoethyl)-1,2-ethanediamine) have been synthesized by reacting $[RuCl_2(PPh_3)_3]$ (**1**) with one mole equivalent of N^1-(2-aminoethyl)-1,2-ethanediamine in dichloromethane Reaction of (**2**) with half-equivalent of $(PhCN)_2PdCl_2$ or $Pd(OAc)_2$ in dichlormethane as a solvent afforded heterotrimetallic Ru–Pd–Ru complexes, $[Ru^{II}Cl_2(PPh_3)_2(\text{triamine})]_2[Pd^{II}X_2]$(X = Cl, OAc) (**3** and **4**). The progress of the undertaken reactions was monitored by $^{31}P\{^1H\}$ NMR and FTIR and the crystal structure of complex 2 was confirmed by X-ray diffraction. Structural analysis revealed that complex 2 crystallizes in the centrosymmetrical P21/c space group with the Ru atom coordinated to two chlorine species in trans form Moreover, the synthesized complexes have been screened for antibacterial activity against *Eschericia coli*, *Bascillus subtilis*, *Pseudomonas aeruginos*, *and Staphylococcus aureus*, as well as for antifungal activity against *Aspergillus niger*, *Candida albicans*, *Fusarium oxysporum and Penicillium sp.*

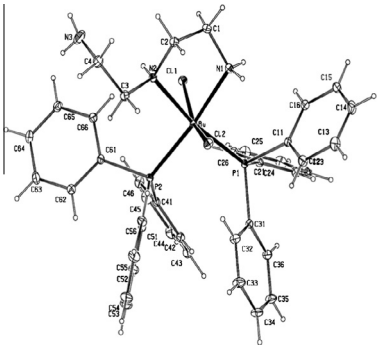

ARTICLE INFO

Article history:
Received 24 September 2013
Received in revised form 19 October 2013

ABSTRACT

New ruthenium(II) mononuclear complexes of the type $[RuCl_2(PPh_3)_2(\eta^2\text{-triamine})]$ (**2**) $[RuCl(PPh_3)_2(\eta^3\text{-triamine})]Cl$ (**5**) (triemine = N^1-(2-aminoethyl)-1,2-ethanediamine) have been synthesized by reacting $[RuCl_2(PPh_3)_3]$ (**1**) with one mole equivalent of N^1-(2-aminoethyl)-1,2-ethanediamine in dichloromethane. Reaction of (**2**) with half-equivalent of $(PhCN)_2PdCl_2$ or $Pd(OAc)_2$ in dichloromethane as a

* Corresponding authors. Tel.: +970 923410003; fax: +962 (5) 3826613.
E-mail addresses: manoaimi@hu.edu.jo (M. Al-Noaimi), warad@najah.edu (I. Warad).

http://dx.doi.org/10.1016/j.saa.2013.11.052

Accepted 10 November 2013
Available online 21 November 2013

Keywords:
Ruthenium(II)/palladium(II) complexes
Triamine
X-ray diffraction
DFT calculation
Antimicrobial activity
Electrochemistry

solvent afforded two novel heterotrimetallic Ru(II)–Pd(II)–Ru(II) complexes, $[Ru^{II}Cl_2(PPh_3)_2(triamine)]_2[Pd^{II}X_2]$(X = Cl, OAc) (**3** and **4**), bearing bioactive ligand. The progress of the undertaken reactions was monitored by $^{31}P\{1H\}$ NMR and FTIR. Crystal structure of complex **2** was confirmed by X-ray diffraction. The absorption spectrum of **2** in dichloromethane was modeled by time-dependent density functional theory (TD-DFT). The *in vitro* antimicrobial studies of complex **2**–**5** against an array of microorganisms (bacteria and fungi) were conducted. Complexes **3** and **4** exhibit high dual antibacterial and antifungal activity inhibiting microorganisms possibly via hydrolytic pathway which further evidenced by electrochemical analyses. The complexes **3** and **4** show a high inhibitory activity at 200 μg/ml concentration, suggesting that complexes **3** and **4** are two efficient catalytic inhibitor of microorganisms and further, they should be tested against cancer strains.

Introduction

Coordination chemistry of ruthenium(II) complexes have been studied in the last few decades because of their versatile and various applications in several fields such as catalysis [1–3], photophysics and photochemistry [4–6], bioinorganic chemistry [7–9] and supramolecular [10–12]. Also, ruthenium complexes containing chloro, dmso and pyridine type ligands [13–15] could be used as chemotherapeutic agents [12]. Ru(II) compounds bearing chelating diphosphine and diamine ligands have received much attention in the last decades due to their application in the field of homogeneous catalysis [15–18]. Also it is possible to increased antimicrobial activity for Ru(II) ion by chelating [19]. Chelating reduces the polarity of the metal atom and enhance the lipophilic character of the central metal atom, which subsequently favors its permeation through the lipid layers of the cell membrane and blocking the metal binding sites on enzymes of microorganism [19–21].

Heteropolymetallic systems have received a great deal of interest over the past decades for their potential applications in catalysis [22], biological systems [23] and molecular magnetism [24]. Palladium (II) mononuclear complexes were used as precursors for the preparation of heterometallic mixed-metal complexes and nanomaterials [25,26]. Vargaftik and coworkers have synthesized a series of heterobimetallic palladium (II)-based lantern-type complexes of the general formula $Pd^{II}M^{II}(\mu\text{-OOCMe})_4L$ (M = Mn, Co, Ni, Zn; L = H_2O, MeCN) [27]. In these complexes the Pd^{II} and M^{II} atoms are drawn together by four acetate bridges, so that the Pd...M distances are close to the sum of covalent radii, thereby implying some metal–metal interaction.

In the present work and as part of our continuous effort to explore the coordination chemistry of Ru(II) mixed-ligand complexes [28–32], new mononuclear $[RuCl_2(PPh_3)_2(\eta^2\text{-triamine})]$ (**2**) and $[RuCl(PPh_3)_2(\eta^2\text{-triamine})]Cl$ (**5**) complexes were synthesized by reacting $[RuCl_2(PPh_3)_3]$ (**1**) with one mole equivalent of N^1-(2-aminoethyl)-1,2-ethanediamine in dichloromethane. In addition, heterotrimetallic, mixed-Ruthenium(II)-Palladium(II) complexes, $[Ru^{II}Cl_2(PPh_3)_2(triamine)]_2\text{-}[Pd^{II}X_2]$ (X = Cl, OAc) (**3** and **4**), were prepared by reaction of $(PhCN)_2PdCl_2$ or $Pd(OAc)_2$ with two equivalents of $[RuCl(PPh_3)_2(\eta^2\text{-triamine})]Cl$ (**2**). Comprehensive characterization of the synthesized complexes has been undertaken by IR, NMR, mass spectra and XRD. The synthesized complexes also have been studied electrochemically and screened for antibacterial and antifungal.

Experimental

Materials

Chemicals were obtained from "Merck" and "B.D.H" Companies. Triphenylphosphine was purchased from Fluka. CH_2Cl_2, n-hexane, and Et_2O were distilled from CaH_2, $LiAlH_4$, and from sodium/benzophenone, respectively. $[RuCl_2(PPh_3)_3]$ complex **1** was prepared according to the published method [33].

*Preparation of complex **2***

N^1-(2-aminoethyl)-1,2-ethanediamine (0.057 ml, 0.58 mmol) ligand was dissolved in 10 mL of dichloromethane and the solution was added dropwise to a stirred solution of $[RuCl_2(PPh_3)_3]$ (**1**) (0.500 g, 0.522 mmol) in 10 mL of dichloromethane. The reaction mixture was stirred approximately for 50 min at room temperature. The brown solution was filtered to remove the insoluble impurities. The solvent was reduced by a vacuum and the product was then precipitated by adding *n*-hexane. The yellow solid was filtered and washed three times with 20 mL of diethyl ether. Crystals suitable for X-ray structural analysis have been obtained by layer-diffusion of diethylether into dichloromethane solutions of the complex. Yield (0.342 g, 82%). M.p is 239–241 °C. IR (KBr, νcm^{-1}): 3330 ($\nu_{Free\ NH2}$), 3276 (ν_{NH2}), 3227 (ν_{NH}). ^1H NMR (CD_2Cl_2, δ ppm): 2.48–4.21 (br, m, 13H, $(H_2NCH_2CH_2)_2NH$), 7.24-7.78 (m, 30H, C_6H_5). $^{31}P\{1H\}$ NMR (CD_2Cl_2): δ (ppm) 44.00 and 43.94 (dd). FAB-MS: 799.2. Anal. Found: C, 60.22; H, 5.28; N, 5.14%. Calc. for $C_{40}H_{43}Cl_2N_3P_2Ru$: C, 60.08; H, 5.42; N, 5.25.

*Preparation of complex (**3**, **4** and **5**)*

Complexes **3** and **4** were prepared by dissolving $(PhCN)_2PdCl_2$ or $Pd(OAc)_2$ (0.1 mmol) in 10 mL of dichloromethane and then the solution was added dropwise to a stirred solution of complex **2** (0.2 mmol) in 10 mL of dichloromethane. The reaction mixture was stirred approximately for 50 min at room temperature. The brown solution was filtered to remove the insoluble impurities. The solvent was reduced by a vacuum and the product was then precipitated by adding *n*-hexane. Complex **5** was prepared by lifting (0.1 g, 0.2 mmol) of complex **2** under stirring for 2 h. Samples were taken during reaction for ^{31}P NMR measurements.

Instrumentation

Infrared (IR) spectra were recorded on Perkin Elemer FTIR spectrometer using KBr disc at room temperature in the range 400–4000 cm^{-1}. Electronic absorption spectra were recorded on a Shimadzu 240-UV–visible spectrophotometer at room temperature. ^1H NMR spectra were recorded on a Bruker DRX 250 spectrometer at 298 K (300 MHz). ^{31}P chemical shifts were measured relative to 85% H3PO4 ($\delta p = 0$). Elemental analysis for carbon, hydrogen and nitrogen were performed on Eurovector E.A.3000 instrument using copper sample-tubes. FAB-MS data were obtained on a Bruker IFS 48 FT-IR spectrometer and Finnigan 711A (8 kV), modified by AMD and reported as mass/charge (m/z), respectively. All electrochemical experiments were done in a

home-built cylindrical vacuum-tight one-compartment cell. A spiral-shaped Pt wire and an Ag wire as the counter and thin pseudo-reference electrodes are sealed into glass capillaries via standard joints and fixed by Quickfit screws. A platinum electrode is introduced as the working electrode through the top central port via a Teflon screw cap with a suitable fitting. It is polished with first 1 μm and then 0.25 μm diamond pastes before measurements. The cell was attached to a conventional Schlenk line via a side arm equipped with a Teflon screw valve and allows experiments to be performed under argon atmosphere with approximately 5 mL of analyte solution. Tetrabutylammonium hexafurophosphate (0.1 M) was twice recrystallized and vacuum dried at 120 °C, and used as the supporting electrolyte. The temperature was controlled (at 25.0 ± 0.1 °C) by a Haake D8-G refrigerator.

X-ray crystallography

Crystals suitable for X-ray structural analysis have been obtained for Ru(II) complex by layer-diffusion of diethylether into dichloromethane solutions of the complex. Selected crystals were mounted on a P4 Siemens diffractometer by using a perfluorinated polyether (Riedel de Haen) as protecting agent. Graphite-monochromated Mo Kα radiation (λ = 0.71073 Å) was used for the measurement of intensity data in the ω-scan mode. The data were corrected for polarization and Lorentz effects. The structure was solved with SHELXS [34] and the refinement was carried out with full-matrix least-squares methods based on F^2 in SHELXL [35] with anisotropic thermal parameters for all non-hydrogen atoms. Hydrogen atoms were included at calculated positions using a riding model; they were located from the difference map.

Computational methods

Full geometry optimization of **1** was carried out using density functional theory (DFT) at the B3LYP level [36]. All calculations were carried out using the GAUSSIAN 03 program package with the aid of the GaussView visualization program [37]. For C, H, Cl, N and P the 6-31G(d) basis set were assigned, while for Ru, the LanL2DZ basis set with effective core potential were employed [38]. Vertical electronic excitations based on B3LYP optimized geometries were computed using the time-dependent density functional theory (TD-DFT) formalism in dichloromethane using conductor-like polarizable continuum model (CPCM) [39–42]. Gauss Sum was used to calculate the fractional contributions of various groups to each molecular orbital [43].

Microbial strains

Gram negative bacteria: *Escherichia coli* (ATCC 25922) and *Pseudomonas aeroginosa* (ATCC 27853), two Gram positive bacteria: *Staphylococcus aureus* (ATCC 25213) and *Bacillus subtilis* (ATCC 6633), and four fungi: *Aspergillus niger* (ATCC 16404), *Candida albicans* (ATCC 10231), *Penicillium digitatum* (ATCC 201167), and *Fusarium oxysporum* (ATCC 11850) were used as microbial strains. Bacterial strains were stocked onto nutrient agar slant and fungal strains were stocked onto malt agar slant. All slants were stored at 4 °C.

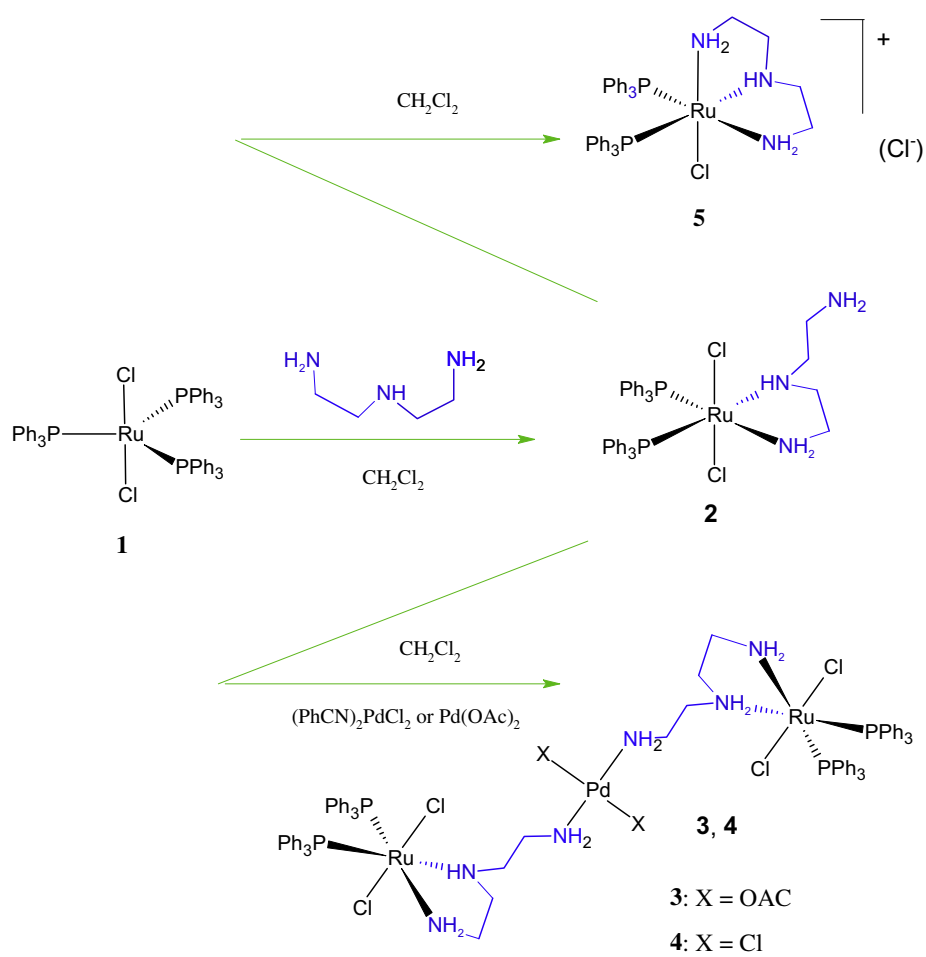

Scheme 1. Synthetic scheme of the complexes **2**–**5**.

Antimicrobial assay

Disc diffusion method [44–45] was used to study the antimicrobial activity of different complexes prepared in this study. Stock compounds were dissolved in DMSO (5 mg/ml) and sterilized using 0.45 μm membrane filters. Sterile 6 mm diameter filter paper discs were loaded with 0.2 mg/disc of each sterile complex and were placed in triplicates onto Muller-Hinton agar (Oxoid, England) plates for bacteria and malt extract agar for fungi. These plates were previously inoculated separately with 100 μL (1.0×10^8 CFU ml^{-1}) of fresh culture of bacteria, fungal spores, or yeast cells suspension. The plates were incubated for 24 h at 37 °C (for bacteria) or for 48–72 h at 28 °C (for fungi). At the end of the incubation time, the diameters of inhibition zone around each of the discs were measured and recorded. Reported inhibition zones are the average calculated from three replicates. Discs soaked with 5%DMSO were used as a negative control. While standard antibacterial tetracycline (30 μg/disc) and antifungal nystatin (100 μg/disc) (Oxoid, Basingstoke, UK) were included as positive controls in the assay.

Results and discussion

Synthesis

Scheme 1 summarizes the reaction pathways for the synthesis of complexes (**2**–**5**). The mononuclear [$RuCl(PPh_3)_2(\eta^2$-triamine)]Cl (**5**) was obtained in a very good yield by the reaction of [$RuCl_2(PPh_3)_3$] (**1**) and one mole equivalent of N^1-(2-aminoethyl)-1,2-ethanediamine in dichloromethane. The mononuclear [$RuCl_2(PPh_3)_2(\eta^2$-triamine)] (**2**) complex was prepared by the substitution one of the labile chloride ligand of complex **5** with stronger amine ligand. Furthermore, the heterotrimetallic, [$Ru^{II}Cl_2(PPh_3)_2$(triamine)]$_2$[$Pd^{II}X_2$] (X = Cl, OAc) (**3** and **4**) complexes were prepared by reaction of $(PhCN)_2PdCl_2$ or $Pd(OAc)_2$ with two equivalents of [$RuCl(PPh_3)_2(\eta^2$-triamine)]Cl (**2**). The free NH_2 belongs to complex **2** coordinated to $Pd(OAc)_2$ or $(PhCN)_2PdCl_2$ in *trans* form to minimize the steric effect. The formation of heterotrimetallic $Ru^{II}/Pd^{II}/Ru^{II}$ complexes was confirmed on the basis of results of elemental analyses, molecular ion peak in FAB-mass spectra, characteristic bands in FT-IR, ^1H, ^{13}C $^{31}P\{1H\}$NMR. The elemental analysis and observed molecular ion peaks at *m/z* 799.2, 1776.2, 1823.3 and 764.3 corresponding to complexes **2**–**5**, respectively, are consistent with the proposed molecular formula of each complex and single crystal XRD in case of complex **2**.

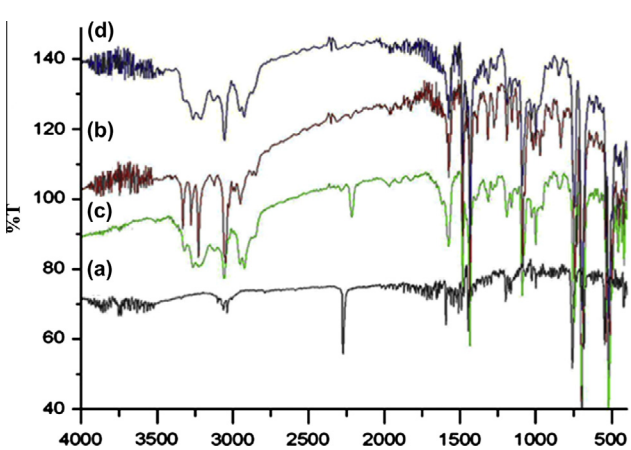

Fig. 1. FT-IR spectra of (a) $(PhCN)_2PdCl_2$, (b) complex **2**, (c) progress of the reaction by using [1:1] mixture of complex **2** and $(PhCN)_2PdCl_2$. (d) IR spectrum for complex **4** which was obtained by reaction of complex **2** mixture of complex **2** and $(PhCN)_2PdCl_2$ in [2:1] mole ratio.

IR spectra

The IR spectrum of complex **2** showed five main sets of characteristic absorptions at 3330, 3276, 3227 cm^{-1}, 3050 and 2860 cm^{-1}, which can be attributed to stretching vibrations free NH_2, NH_2, NH, and Ph-H, CH_2 function groups respectively. The presence of ruthenium bound PPh_3 is indicated by three strong bands at ~745, ~694 and ~516 cm^{-1} respectively.

The reaction between complex **2** and $(PhCN)_2PdCl_2$ in CH_2Cl_2 to form heterotrimetallic [$Ru^{II}Cl_2(PPh_3)_2$(triamine)]$_2$[$Pd^{II}Cl_2$] (**4**) was monitored by IR. Fig. 1a shows the ν(C≡N) of the $(PhCN)_2PdCl_2$ complex at 2260 cm^{-1}. This band loses its intensity by stepwise addition of complex **2** (Fig. 1b) to $(PhCN)_2PdCl_2$. Using [1:1] mole ratio of complex **2** to $(PhCN)_2PdCl_2$ causes replacement of one of the labile PhCN of $(PhCN)_2PdCl_2$ moieties with the much stronger amine ligand, thereby decreasing the intensity of the C≡N band at 2260 cm^{-1} to almost one-half of its initial value (Fig. 1c). When the ratio reach a value of [2:1], a complete substitution of the second PhCN occured and the disappearance of the ν(C≡N) band was a strong evidence for formation of complex **5** (Fig. 1d).

^1H NMR and ^{13}C NMR spectra

^1H NMR spectra of complexes **2** and **5** showed a broad signal at δ = 2–4.2 ppm, which has been attributed to hydrogens of triamine co-ligand. The aromatic protons for the coordinated triphenyphosphines appeared at δ = 6.8–8.7 ppm as broad signals. In case of complexes **3** and **4**, all signals observed for hydrogen were in their excepted region. In addition, the spectra contain also a broad signal at δ = 2.6 ppm, which can be assigned to (6H) for the acetate group (CH_3COO) of complex **3**.

^{31}P NMR spectra

The formation of complexes **5** and **3** form complex **2** was monitored by ^{31}P NMR spectra. Complex **2** (Fig. 2a) exhibits two doublets around 44.00 and 43.94 ppm with J*pp* = 35.3, which are assigned to the two non-identical phosphorus atoms. After 1 h (Fig. 2b) and 2 h (Fig. 2c) from dissolving and stirring the complex in CD_2Cl_2 at room temperature, the intensity of the two peaks at 40.1 and 43.9 ppm started to decrease by decreasing the amount of complex **2** and the appearance of two new doublets with AB $^{31}P\{^1H\}$ NMR pattern at 43.4, 47.5 ppm (J*pp* = 38.2 Hz) (Fig. 2b and c) by increasing the amount of complex **5**. After 3 h (Fig. 2d), the two doublet at 40.1 and 43.9 ppm completely disappeared and there is only two doublets at 43.4 and 47.5 ppm. Significantly, the chemical shift and the P-P coupling constant of the phosphine ligand in $^{31}P\{^1H\}$ NMR clearly confirmed the completion of the reaction and there was only one product which is complex **5**.

Stepwise formation of complex **3** from complex **2** with time in a stirred solution of dichloromethane was monitored by $^{31}P\{^1H\}$ NMR as illustrated in Fig. 3. Fig. 3a shows $^{31}P\{^1H\}$ NMR Complex **2.** 10 min after addition of $Pd(OAc)_2$ the two doublets of complex **2** (44.00 and 43.94 ppm with J*pp* = 35.3) (Fig. 3b) started to disappear and new two doublets at δ (ppm) 38.3 and 45.1 (dd) with J*pp* = 35.3,) for complex 3 started to appear. After 40 min, the reaction was completed (Fig. 3c) with the disappearance of the two doublets of complex **2** and the remaining of the two doublets of complex **3**. 2 h later the two doublets of complex **3** started to disappear and a new singlet at 43.9 ppm for the free PPh_3 ligand started to appear as an indication for the decomposition of the complex (Fig. 3d).

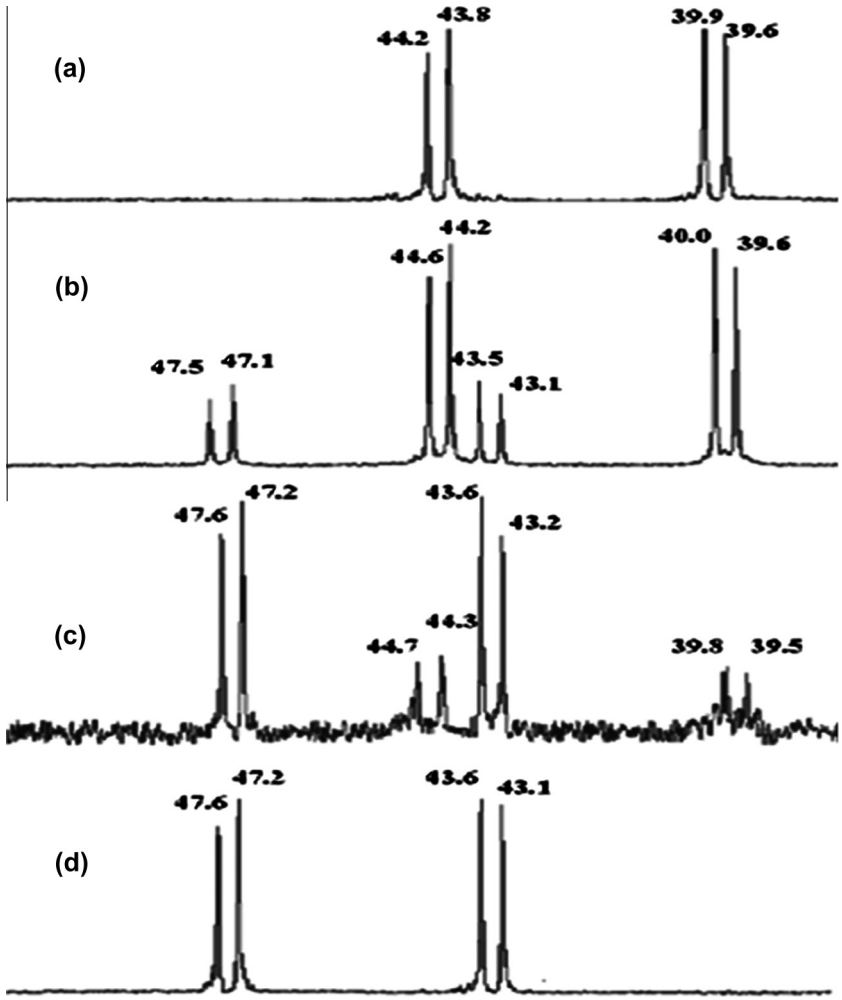

Fig. 2. (a) $^{31}P\{^{1}H\}$ NMR spectroscopic complex **2** in $CDCl_3$, (b) progress of the reaction after 1 h, (c) after 2 h and (d) after 3 h.

*Crystal structure of complex **2***

X-ray crystal structure of complex **2** was obtained and the molecular structure is shown in Fig. 4. Their main crystallographic data are reported in Table 1, while some selected bond lengths and angles are given in Table 2. Complex **2** crystallizes in the centrosymmetrical *P*21/*c* space group. The ruthenium atom is coordinated in a distorted octahedral with two chlorides are in a *trans* form, one diamine co-ligand *via* the two nitrogen (N(1) and N(2)) atoms and two PPh_3 ligands *via* the (P(1) and P(2)), as in scheme 1. The two chloride ligands are bent away from their axial positions toward the diamine ligand due to steric factor of the phosphines phenyls, forming Cl–Ru–Cl angles of 161.67°. The chelating bit angle for N(1)–Ru(1)–N(2) is 78.75(9) while the P–Ru–P angle of 94.40(2). The Ru(1)–N(1) (2.161(2) Å) bond length is shorter than Ru(1)–N(2) (2.225(2) Å) due to the free rotation of the unchelating free alkylamine.

UV–visible studies

UV–visible electronic absorption spectrum of complex **2** was measured in dichloromethane. The electronic absorption spectra of **2**–**5** are very similar, all have two weak absorption bands around 450–430 nm with a molar absorption coefficient of the order of 10^2 M^{-1} cm^{-1}, and intense high energy absorption around 310–340 nm. Complex **2** as a representative example (Fig. 5) has two bands, weak transitions around $\lambda = 445$ and a strong transition around 315 nm.

The electronic transitions for complex **2** in dichloromethane have been assigned based on the DFT and TDDFT calculation. The optimized structure of this molecule is developed using GAUSSIAN 03 analyses package [37]. The structural agreement has been observed from the comparison of bond distances and angles between calculated and X-ray determined structure (Table 2). The DFT calculated values for the bond angles were in closest agreement. The orbital energies along with contributions from the ligands and metal are given in Table 3 which depicts selected occupied and unoccupied frontier orbitals. Moreover, the isodensity plots for the HOMOs and LUMOs orbitals for complex **1** are shown in Fig. 6. The HOMO to HOMO−2 is constituted by >75% contribution from Ru where is HOMO−3 to HOMO−10 are mainly PPh_3 in character. The LUMO is composed of 55% Ru and 23% of PPh_3 ligand. This large contbution from the metal d-orbital in the LUMO suggests a significant back donation [46] from the Ru(dπ) → P(dπ)). LUMO+ is composed from 24% from Ru and 76% from diphosphine ligand. LUMO+1 to LUMO+10 are composed mainly from PPh_3 ligands.

The full theoretical absorption spectra were obtained from the calculation of the singlet excited states with TD-DFT using B3LYP functional and a mixed basis set, LanL2DZ/6-31+G(d,p), in dichloromethane as a solvent via polarized continuum model (PCM). Computation of 40 excited states of complex **1** allowed the interpretation of the experimental spectra in the 300–800 nm range

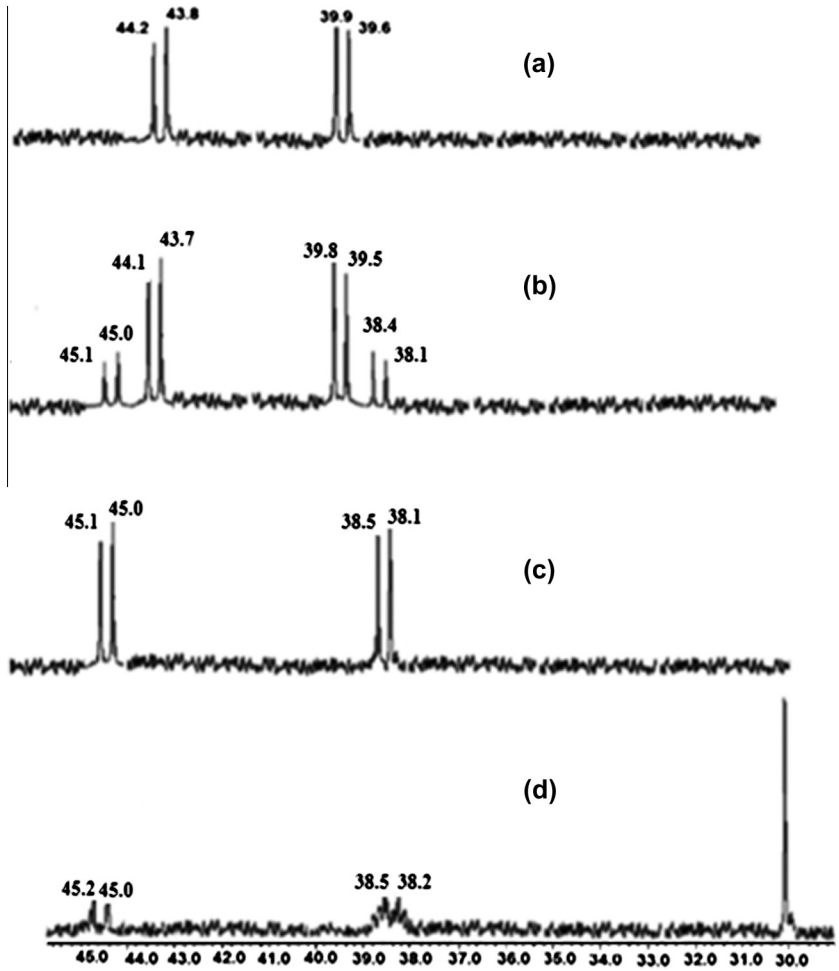

Fig. 3. $^{31}P\{^1H\}$ NMR spectra: (a) pure complex **2**, (b) complex **2** after 10 min from $Pd(OAc)_2$ addition, (c) pure complex **3** (after 40 min), and (d) complex **3** (after 2 h) the complex start to decomposed.

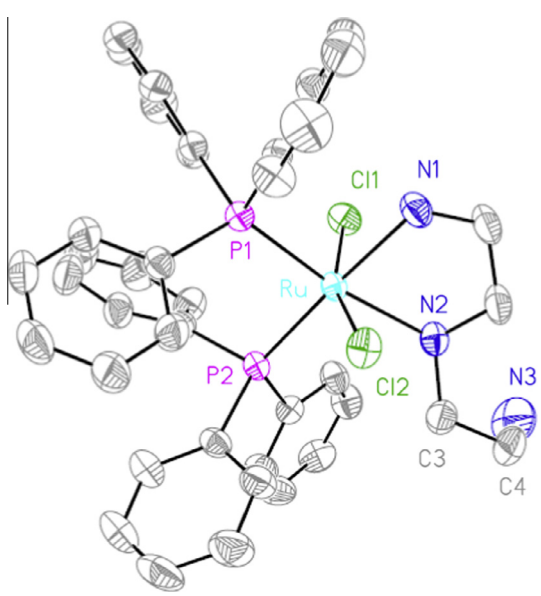

Fig. 4. ORTEP drawing of complex **2**.

Table 1
Crystal data and structure refinement for the complex **2**.

Empirical formula	$C_{40}H_{43}Cl_2\ P_3P_2Ru$
Formula weight	799.7
Crystal size (mm)	0.6 × 0.4 × 0.3
Crystal description	Orange–brown block
Temperature	293(2) K
a = 10.2188(16) (Å)	α = 90 (°)
b = 17.850(3) (Å)	B = 98.95(3) (°)
c = 20.393(5) (Å)	γ = 90 (°)
Volume (Å)	3674.5(12)
Crystal system	Monoclinic
Space group	$P21/c$
Z	4
Density (calculated) mg/m^3	1.446
Absorption coefficient (mm^{-1})	0.693
$F(000)$	1648
θ range for data collection (°)	3.05–25.97
θ range (lattice) (°)	8.061–12.282
Index ranges	$-12 \leqslant h \leqslant 12$, $0 \leqslant k \leqslant 21$, $-1 \leqslant l \leqslant 25$
Reflections collected	7806
Independent reflections	7183 [R_{int} 0.0254]
Absorption correction	Psi-Scans
Refinement method	Full-matrix least-squares on F^2
Data/restraints/parameters	7183/0/453
Goodness-of-fit on F^2	1.030
Final R indices [$I > 2\gamma$ (I)], R_1/wR_2	0.0299/0.0639
R indices (all data), R_1/wR_2	0.0506/0.0698
CCDC	948767

Table 2
Selected bond lengths (Å) and bond angles (°) for the complex **2**.

Bond length (Å)		
Experimental calculated		
Ru(1)–Cl(1)	2.404(8)	2.576
Ru(1)–Cl(2)	2.435(5)	2.541
Ru(1)–P(1)	2.328(7)	2.527
Ru(1)–P(2)	2.340(10)	2.529
Ru(1)–N(1)	2.161(2)	2.201
Ru(1)–N(2)	2.225(2)	2.144
Bond angel [deg]		
Cl(1)–Ru(1)–Cl(2)	161.67(2)	163.23
P(1)–Ru(1)–P(2)	94.40(2)	92.05
N(1)–Ru(1)–N(2)	78.75(9)	79.68
N(1)–Ru(1)–Cl(1)	82.54(8)	85.63
N(2)–Ru(1)–Cl(1)	85.65(7)	87.89
N(1)–Ru(1)–Cl(2)	81.03(8)	83.25
N(2)–Ru(1)–Cl(2)	83.22(7)	85.32
N(1)–Ru(1)–P(1)	90.59(7)	89.25
N(2)–Ru(1)–P(1)	168.74(6)	169.98
N(1)–Ru(1)–P(2)	173.46(7)	175.23
N(2)–Ru(1)–P(2)	96.51(6)	93.36
P(1)–Ru(1)–Cl(1)	96.63(3)	93.82
P(2)–Ru(1)–Cl(1)	92.67(3)	91.09
P(1)–Ru(1)–Cl(2)	91.63(3)	90.25

Table 3
DFT energies and composition of selected highest occupied and lowest unoccupied molecular orbitals of complex **2** expressed in terms of composing fragments.

	eV	Ru	pph_3	en	Cl
LUMO+10	−0.17	1	98	1	0
LUMO+9	−0.22	1	98	1	0
LUMO+8	−0.33	3	96	0	1
LUMO+7	−0.34	1	98	1	0
LUMO+6	−0.43	9	88	1	2
LUMO+5	−0.48	4	95	1	0
LUMO+4	−0.51	3	97	0	0
LUMO+3	−0.72	12	84	4	0
LUMO+2	−0.77	3	96	1	1
LUMO+1	−0.89	13	83	4	0
LUMO	−1.02	55	23	5	16
HOMO	−5.18	75	3	2	20
HOMO−1	−5.21	76	4	1	20
HOMO−2	−5.62	87	10	3	0
HOMO−3	−6.21	1	1	96	1
HOMO−4	−6.43	5	80	5	10
HOMO−5	−6.46	5	71	8	15
HOMO−6	−6.68	1	92	1	6
HOMO−7	−6.7	2	86	1	12
HOMO−8	−6.73	1	96	0	3
HOMO−9	−6.77	1	93	1	5
HOMO−10	−6.82	2	81	1	16

(Fig. 5). The calculated energy of excitation states and transition oscillator strength (*f*) are shown in Table 4. The absorption spectrum of **1** was simulated using Gaussian Sum software [43] based on the obtained TD-DFT results. Both the experimental UV/visible spectrum of complex **1** reported in dichloromethane and its simulated absorption spectrum shown in Fig. 6 were in acceptable agreement. On the basis of its intensity and position, a weak broad band at 445 nm (≈420 (calculated)) resulted from HOMO−2 → LUMO (86%) thus band is assigned to d-d (t_2(Ru) → e(Ru))transition [46]. The broad high-energy band at 330 composed from the overlap of two transition (≈291 nm (calculated)) nm which is resulted from HOMO−1 → LUMO + 7 (21%), HOMO−1 → LUMO + 8 (60%) and assigned as MLCT (t_2(Ru) → P(dπ)) and (270 nm(calculated)) which is resulted from HOMO−5 → LUMO (68%) and assigned to ligand–ligand charge transfer π → π (P(dπ) → P(dπ)) charge transfer transitions [47].

Electrochemistry

Cyclic voltammetry of complex **2** as a representative example was examined in acetonitrile solution containing $[Bu_4N][PF_6]$ as the supporting electrolyte (Fig. 7). Complex **2** exhibits a quasi-reversible oxidation wave at $E^0 = 0.27$ V vs Ag/Ag^+. Scanning the potential to very positive and negative potentials (−2 V to +2 V) did not show any additional processes. Thus, the quasi-reversible oxidation wave 0.27 V is assigned to $Ru^{III/II}$ couple. The diffusion coefficient (D) of **2** is determined under these conditions and a

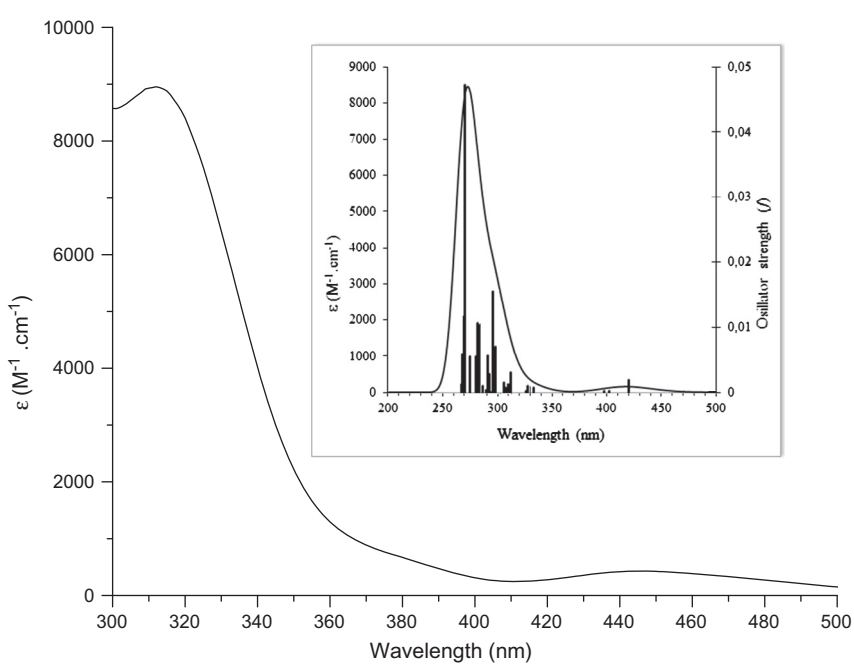

Fig. 5. UV–visible spectrum for **2** in dichloromethane. Inset shows simulated absorption spectrum. (black line) based on TD-DFT calculations, compared to excitation energies and oscillator strengths.

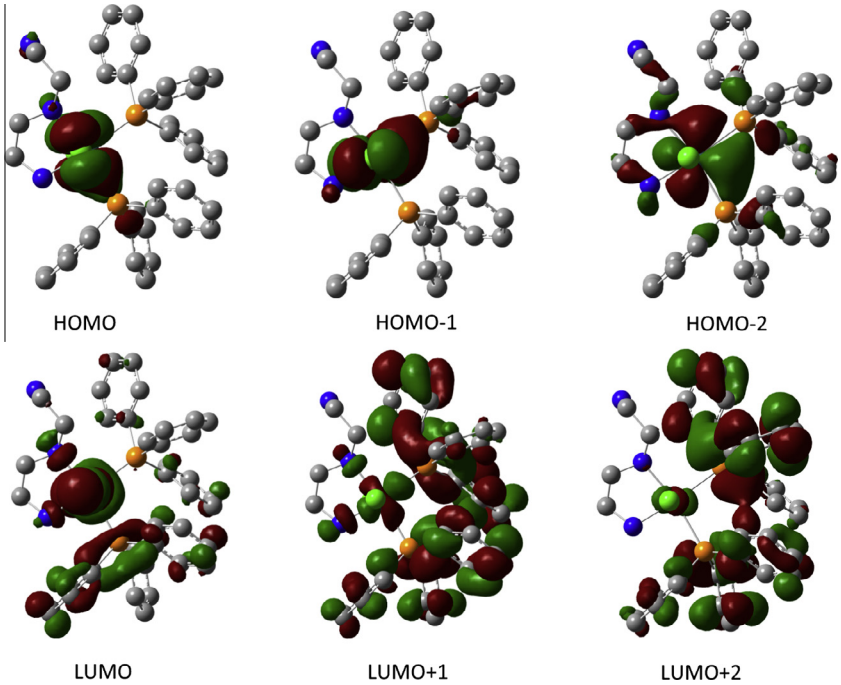

Fig. 6. Isodensity plots of the HOMO and LUMO orbitals of **1**.

Table 4
Computed excitation energies (nm), electronic transition configurations and oscillator strengths (f) for the optical transitions in the visible region of complex **2** transitions with oscillator strength $f \geqslant 0.0019$ are listed).

nm	eV	f	Major contribs
420.3	2.96	0.0019	HOMO−2- > LUMO (86%)
295.1	4.21	0.0155	HOMO−2 → LUMO+2 (86%)
292.1	4.25	0.0028	HOMO → LUMO+7 (85%), HOMO → LUMO+8 (11%)
291.0	4.27	0.0056	HOMO−1 → LUMO+7 (21%), HOMO−1 → LUMO+8 (60%)
281.8	4.41	0.0019	HOMO−1 → LUMO+9 (79%)
279.1	4.45	0.0103	HOMO−2 → LUMO+4 (52%), HOMO−2 → LUMO+5 (19%)
278.0	4.47	0.0073	HOMO → LUMO+10 (56%)
276.6	4.49	0.0032	HOMO−1 → LUMO+10 (49%)
276.4	4.50	0.0106	HOMO−2 → LUMO+6 (30%), HOMO−1 → LUMO+10 (20%)
270.4	4.59	0.0472	HOMO−5 → LUMO (68%)
270.1	4.60	0.0108	HOMO → LUMO+11 (76%)
269.5	4.61	0.0116	HOMO−4 → LUMO (48%), HOMO−3 → LUMO (34%)
268.4	4.63	0.0059	HOMO−4 → LUMO (16%), HOMO−3 → LUMO (51%)

Table 5
Antimicrobial activity (mm inhibition zone diameter) of 0.2 mg/ml complexes **2**–**4**.

Compd.	Bacterial strains [a] (Inhibition zone diameter in mm)				Fungal strains [b] (Inhibition zone diameter in mm)			
	(A)	(B)	(C)	(D)	(E)	(F)	(G)	(H)
2	16.2	12.9	11.0	15.5	13.6	22.5	20.5	12.4
3	22.4	21.2	19.5	22.6	27.5	24.5	19.0	15.0
4	22.5	21.5	19.0	22.3	27.1	24.8	20.4	16.2
TTCN [c]	20.0	24.7	18.5	25.8	–	–	–	–
NST [d]	–	–	–	–	28.0	33.7	25.5	20.8

[a] (A): *E. Coli*; (B): *Staphylococcus aureus*; (C): *Pseudomonas aeroginosa*; (D): *Bacillus subtilis*.
[b] (E): *Aspergillus niger*; (F): *Candida albicans*; (G): *Penicillium digitatum*; (H): *Fusarium oxysporum*.
[c] TTCN: Tetracycline.
[d] NST: Nystatin.

value of 5.35×10^{-6} cm^2 s^{-1} was estimated by using the Randles–Sevcik equation [48]. In spite of the long term stability of compound **2**, attempts to electrochemically oxidize the other complexes **3**, **4** and **5** have failed due to their rapid decomposition under the oxidative conditions. This is probably due to their solvolysis by CH_3CN.

*Antimicrobial activity of complexes **2–4***

The complexes produced in this study showed different activities against an array of Gram positive, Gram negative bacteria and fungi. All the three complexes exhibited high antifungal activity against *C. albicans* and *P. digitatum* with inhibition zones above 19 mm (Table 3). Complex (**2**) showed a weak to moderate antifungal activity against *A. niger* and *F. oxysporum* with inhibition zones less than 14 mm. In contrast, the two new trimetallic complexes (**3**) and (**4**) showed a significant activity against all fungal strains except *F. oxysporum* where a moderate activity (inhibition zone < 16.5) was observed. Surprisingly, no activity was observed for compounds **5** against all tested strains (Table 5). All bacterial strains were significantly inhibited by complex **3** and **4** with inhibition zones above 19 mm. complex **2** exhibited moderate activity against *E. coli* and *B. subtilis* with inhibition zones of 16.2 and 15.5 mm, respectively. The antibacterial and antifungal activity results were compared respectively with those reported for standard drugs such as Tetracycline (TTCN) and Nystatin (NST) as shown in (Table 5). It is also known that Ru complexes that have Ru–$(aquo)_2$ moiety have high biological activities compared to the analogous Ru–$(Cl)_2$ complexes [49]. The high biological activities for the Ru–(Cl) complexes (**2**–**4**) can be explained by the rate of the hydrolysis for Ru–$(Cl)_2$ moiety in the presence of enzymes of microorganisms. During the hydrolysis many metal-aquo//metal-hydroxyl and/or metal-Oxo biological active moieties can be produced. All these species can contribute in oxygen transfer from the complexes to unsaturated organic molecules or bio-targets and cause damage of vital cycle of microorganisms and cancer cells [50–54].

Previous studies showed that many compounds are more active against Gram positive bacteria compared than Gram negative bacteria [55]. However, in our study, complexes **3** and **4** were active against both Gram positive and Gram negative bacteria (Table 5) and it is worthy to report that among the bacteria tested are *S. aureus* and *E. coli*, which are frequently implicated in food poisoning. Such activity of our complexes may be a result of the broad spectrum antibacterial action or general metabolic toxicity [56]. Both possibilities need further investigation using specific biochemical tests.

Due to the high toxicity and limited activity of the commonly used antifungal agents [57] there is a need for the development of new compounds with antifungal potential. In this context, our complexes were active against different fungal strains and have the potential to be considered for possible application as antifungal agents (Table 5). However, the cytotoxicity of both complexes **3** and **4** should be screened on a panel of human normal and cancer cell lines which will reveal if they have a better prospect of acting as a cancer chemotherapeutic agent, and to elucidate the mechanism of tumor/bacteria/fungus inhibition. Furthermore, molecular modeling studies should be carried out to understand molecular features important for drug–enzyme interactions which will offer new insights into the experimental model observations [58].

Conclusion

Two novel mononuclear ruthenium complexes (**2** and **5**) and two heterotrimetallic $Ru^{II}/Pd^{II}/Ru^{II}$ complexes (**3** and **4**) were synthesized. The formation of these complexes was monitored by ^{31}P, $\{^{1}H\}$ and FTIR. The crystal structure of complex **2** is also obtained and confirmed by XRD. The electronic absorption spectra of these complexes showed weak band in the visible region which was assigned to d–d transition and strong broad band in the UV region which was resulted from the overlap of the MLCT and $\pi \rightarrow \pi^*$ transitions. The biological activities of all complexes were examined by screening their ability to inhibit the growth of different bacteria and fungi. Results suggested that complexes **3** and **4** (Ru/Pd) are highly effective compared to complex **2**, whereas complex **5** did not show any detectable activity. The enhanced biological activity of these complexes can be explained on the basis of Overtone's concept and catalytic oxygen transfer.

Acknowledgements

Authors are thankful to the Deanship of Scientific Research, King Saud University Riyadh for funding the work through the research Project No. RGP-VPP_236.

Appendix A. Supplementary material

Supplementary data associated with this article can be found, in the online version, at http://dx.doi.org/10.1016/j.saa.2013.11.052.

References

[1] S.I. Murahashi, Ruthenium in Organic Synthesis, Wiley-VCH, Weinheim, 2004.
[2] B. Deb, P.P. Sarmah, D.K. Datta, Eur. J. Inorg. Chem. (2010) 1710–1716.
[3] M. Pagliaro, S. Campestrini, R. Ciriminna, Chem. Soc. Rev. 34 (2005) 837–845.
[4] W. Henry, C.G. Coates, C. Brady, K.L. Ronayne, P. Matousek, M. Towrie, S.W. Botchway, A.W. Parker, J.G. Vos, W.R. Browne, J.J. McGarvey, J. Phys. Chem. A 112 (2008) 4537–4544.
[5] L. Hammarstrőm, O. Johansson, Coord. Chem. Rev. 254 (2010) 2546–2559.
[6] Y. Sun, S.N. Collins, L.E. Joyce, C. Turro, Inorg. Chem. 49 (2010) 4257–4262.
[7] W.H. Ang, P.J. Dyson, Eur. J. Inorg. Chem. (2006) 4003–4018.
[8] S.H. van Rijt, P.J. Sadler, Drug Discovery Today 14 (2009) 1089–1097.
[9] G. Süss-fink, *Dalton Trans.* 39 (2010) 1673–1688.
[10] F.F. de Biani, E. Grigiotti, F. Laschi, P. Zanello, A. Juris, L. Prodi, K.S. Chichak, N.R. Branda, Inorg. Chem. 47 (2008) 5425–5440.
[11] V. Balzani, G. Bergamini, F. Marchioni, P. Ceroni, Coord. Chem. Rev. 250 (2006) 1254–1266.
[12] D.L. Ma, C.M. Che, F.M. Siu, Inorg. Chem. 46 (2007) 740–749.
[13] A.H. Velders, A. Bergamo, E. Alessio, E. Zangrando, J.G. Haasnoot, C. Casarsa, M. Cocchietto, S. Zorzet, G. Sava, J. Med. Chem. 47 (2004) 1110–1121.
[14] I. Bratsos, B. Serli, E. Zangrando, N. Katsaros, E. Alessio, Inorg. Chem. 46 (2007) 975–992.
[15] M. Toyama, K. Inoue, S. Iwamatsu, N. Nagao, Bull. Chem. Soc. Japan 79 (2006) 1525–1534.
[16] M.P.D. Araujo, A.T. de Figueiredo, A.L. Bogado, G. Von Poelhsitz, J. Ellena, E.E. Castellano, C.L. Donnici, J.V. Comasseto, A.A. Batista, Organometallics 24 (2005) 6159–6168.
[17] S.E. Clapham, A. Hadzovic, R.H. Morris, Coord. Chem. Rev. 248 (2004) 2201–2237.
[18] E. Lindner, H.A. Mayor, I. Warad, K. Eichele, J. Organomet. Chem. 665 (2003) 176–185.
[19] A.H. Collins (Ed.), Microbiology Method, 2nd ed., Butterworth, London, 1976.
[20] B.G. Tweedy, Phytopathology 55 (1964) 910–917.
[21] S.C. Singh Jadon, N. Gupta, R.V. Singh, Ind. J. Chem. 34 (1995) 733–736.
[22] S. Cenini, E. Galloa, A. Caselli, F. Ragaini, S. Fantauzzi, C. Piangiolino, Coord. Chem. Rev. 250 (2006) 1234–1235.
[23] J.N. Chan, Z.Y. Huang, M.E. Merrifield, M.T. Salgado, M.J. Stillman, Coord. Chem. Rev. 233 (2002) 319–339.
[24] O. Kahn, Struct. Bond. 68 (1987) 89–167.
[25] J.M. Thomas, W.J. Thomas, Principles and Practice of Heterogeneous Catalysis, VCH, New York, 1997.
[26] J.H. Sinfelt, Bimetallic Catalysts, Discoveries, Concepts and Applications, Wiley, New York, 1983.
[27] N.Y. Kozitsyna, S.E. Nefedov, F.M. Dolgushin, N.V. Cherkashina, M.N. Vargaftik, I.I. Moiseev, Inorg. Chim. Acta 359 (2006) 2072–2086.
[28] I. Warad, M. Al-Noaimi, O.S. Abdel-Rahman, F.F. Awwadi, B. Hammouti, T.B. Hadda, Spectrochim. Acta Part A Mol. Biomol. Spectrosc. 117 (2014) 250–258.
[29] I. Warad, M. Al-Noaimi, O.S. Abdel-Rahman, M. AlDamen, B. Hammouti, T.B. Hadda, Polyhedron 63 (2013) 182–188.
[30] I. Warad, H. Al-Hussen, H. Alanazi, R. Mahfouz, B. Hammouti, M. Al-Dosari, R. Al-Far, T.B. Hadda, Spectrochim. Acta A 105 (2013) 466–474.
[31] M. Al-Noaimi, M. Sunjuk, M. El-khateeb, S.F. Haddad, A. Haniyeh, M. AlDamen, Polyhedron 42 (2012) 66–73.
[32] I. Warad, E. Lindner, K. Eichele, H.A. Mayor, Inorg. Chim. Acta 357 (2004) 1847–1853.
[33] T.A. Stephenson, G. Wilkinson, Inorg. Nucl. Chem. 28 (1966) 945–950.
[34] G.M. Sheldrick, SHELXS-90, University of Göttingen, Germany, 1990.
[35] G.M. Sheldrick, SHELXS-97, University of Göttingen, Germany, 1997.
[36] C. Lee, W. Yang, R.G. Parr, Phys. Rev. B 37 (1988) 785–789.
[37] M.J. Frisch et al., Gaussian 03, Revision D.01, Gaussian Inc., Wallingford CT, 2004GaussView3.0, Gaussian: Pittsburgh, PA.
[38] P.J. Hay, W.R. Wadt, J. Chem. Phys. 82 (1985) 270–283.

[39] R. Bauernschmitt, R. Ahlrichs, Chem. Phys. Lett. 256 (1996) 454–464.
[40] M.K. Casida, C. Jamorski, K.C. Casida, D.R. Salahub, J. Chem. Phys. 108 (1998) 4439–4449.
[41] R.E. Stratmann, G.E. Scuseria, M.J. Frisch, J. Chem. Phys. 109 (1998) 8218–8224.
[42] M. Cossi, N. Rega, G. Scalmani, V. Barone, Comput. Chem. 24 (2003) 669–681.
[43] N.M. O'Boyle, A.L. Tenderholt, K.M. Langner, J. Comput. Chem. 29 (2008) 839–845.
[44] J.K. Hurst, Coord. Chem. Rev. 249 (2005) 313–328.
[45] D. Chatterjee, A. Mitra, R.E. Shepherd, Inorg. Chim. Acta 357 (2004) 980–990.
[46] S.I. Gorelsky, A.B. Lever, M. Ebadi, Coord. Chem. Rev. 230 (2002) 97–105.
[47] D.M. Massen, G.A. Crosby, J. Mol. Spectrosc. 25 (1968) 398–405.
[48] P. Zanello, Inorganic Electrochemistry: Theory, Practice and Application, The Royal Society of Chemistry, 2003.
[49] T.B. Hadda, M. Akkurt, M.F. Baba, M. Daoudi, B. Bennani, A. Kerbal, Z.H. Chohan, J. Enz. Inhib. Med. Chem. 24 (2009) 457–463.
[50] N. Chanda, B. Mondal, V.G. Puranik, G.K. Lahiri, Polyhedron 21 (2002) 2033–2043.
[51] D. Chatterjee, A. Mitra, S. Mukherjee, J. Mol. Catal. A: Chem. 1654 (2001) 295–298.
[52] D. Chatterjee, A. Mitra, Inorg. Chem. Comm. 3 (2000) 640–644.
[53] D. Chatterjee, A. Mitra, G.S. De, Platinum Metals Rev. 50 (2006) 2–12.
[54] B. Bottari, R. Maccari, F. Monforte, R. Ottanà, E. Rotondo, M.G. Vigorita, Bioorg. Med. Chem. Lett. 10 (2000) 657–660.
[55] A.R. McCutcheon, S.M. Ellis, R.E.W. Hancock, G.H.N. Towers, J. Ethnopharmacol. 37 (1992) 213–223.
[56] D. Srinivasan, S. Nathan, T. Suresh, P. Lakshmana, Perumalsamy, J. Ethnopharmacol. 74 (2001) 217–220.
[57] E.J. Helmerhorst, I.M. Reijnders, W. van't Hof, I. Simoons-Smit, E.C.J. Veerman, A.V.N. Amerongen, Agents Chemother 43 (1999) 702–704.
[58] S. Tabassum, M. Zaki, M. Afzal, F. Arjmand, Dalton Trans. 42 (2013) 10029–10041.